Nanostructured Polymer Films with Liquid Inclusions. 1. Structural Blocks

Olga Kalinina and Eugenia Kumacheva*

Department of Chemistry, University of Toronto, Toronto, Ontario M5S 3H6, Canada

Received February 26, 2001; Revised Manuscript Received June 8, 2001

ABSTRACT: We report the synthesis of core−shell latex particles with liquid cores and rigid shells for use as structural units in the fabrication of polymer nanostructured materials with liquid inclusions. Core- and shell-forming polymers were synthesized from the copolymers of poly(butyl acrylate) (PBA) and poly(methyl methacrylate) (PMMA) with different weight ratios PBA/PMMA in the latex core and shell. The morphology of the core−shell latex particles with fluid cores and rigid shells was examined as a function of the composition of the shell-forming polymer, the weight ratio core-forming polymer/shell-forming polymer in the composite particle, and the concentration of the cross-linking agent in the shell-forming polymer. The optimum conditions were found, under which free of defects monodispersed core−shell particles could be obtained. Factors leading to the collapse of the core−shell particle are discussed and evaluated.

Introduction

Recently, we have proposed a new approach to producing a nanocomposite polymer material with a periodic structure and function, which employed core−shell latex particles.[1] The essential feature of the core−shell microspheres was a specific relation between the glass transition temperatures of the core-forming polymer (CFP) and the shell-forming polymer (SFP); i.e., the glass transition temperature, T_g, of the SFP was substantially lower than that of the CFP. Following synthesis, the core−shell particles were assembled into an ordered close-packed three-dimensional array[2] and heated at the annealing temperature, T_{ann}, under conditions $T_{g,SFP} < T_{annealing} < T_{g,CFP}$. During heat processing, the SFP flowed and ultimately formed a continuous matrix, while the CFP remained intact and produced the dispersed phase of the polymer nanocomposite. The proposed method provided control over particle dimensions and number density in the nanostructured material and enabled us to produce polymeric materials with periodically modulated compositions and properties. For example, by incorporating fluorescent species either into latex cores[1] or into shells,[3] nanostructured polymers with periodically changing optical properties were obtained, which is the intrinsic feature of photonic crystals. We demonstrated that local two-photon-induced photobleaching of individual fluorescent beads which were embedded into an optically inert matrix can be used in optical three-dimensional bitlike memory storage.[4] Other areas of potential applications of polymer nanocomposites with periodically modulated optical properties include optical limiters and switches and display devices.

In such systems, the speed of the optical response of dyes or chromophores localized in the CFP and/or SFP will strongly depend on the physical state of the polymer. Preliminary results obtained in our group on photobleaching of a fluorescent NBD dye incorporated in a low-T_g polymer showed a substantially higher speed of photobleaching of the dye than when it was mixed with a high-T_g polymer. These results are consistent with the findings of Atvars et al.,[5] who have showed that the efficiency of the photobleaching process of fluorescein dissolved in poly(vinyl alcohol) increases above the glass transition temperature of the polymer. The speed factor motivated us to expand the "core−shell" approach to producing polymeric nanocomposites with liquid inclusions, i.e., the materials in which the fluid particles of a low-T_g polymer would be periodically embedded in a matrix formed by a high-T_g polymer.

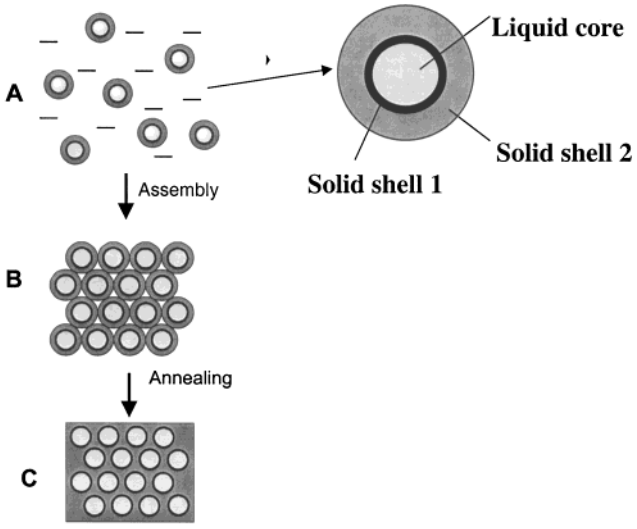

Figure 1. (a) Schematics of the modified "core−shell" approach. (b) Individual particle with a liquid core (A), solid shell 1 (B), and solid shell 2 (C). The relationship between the glass transition temperatures of the CFP, SFP1, and SFP2 is $T_{g,CFP} < T_{room}$; $T_{g,SFP1} > T_{g,SFP2} > T_{g,CFP}$; $T_{g,SFP2} > T_{room}$; $T_{g,SFP2} < T_{ann} < T_{g,SFP1}$.

Figure 1 shows the schematics of the modified core−shell approach. In the first step, three-layer composite latex particles are synthesized, in which the CFP is a low-T_g polymer. The core is coated with two shells synthesized from high-T_g polymers SFP1 and SFP2, respectively. The relationships between the glass transition temperatures of the CFP, SFP1, and SFP2 are $T_{g,CFP} < T_{room}$; $T_{g,SFP1} > T_{g,SFP2} > T_{g,CFP}$; and $T_{g,SFP2} > T_{room}$. In the second step, the composite particles are assembled in 1-, 2-, or 3-dimensional arrays via sedimentation, filtration, capillary flow, or electrodeposition

10.1021/ma0103472 CCC: $20.00
Published on Web 08/03/2001

and then dried. In the third step, the particle array is heat processed at annealing temperature $T_{g,SFP1} < T_{ann} < T_{g,SFP2}$. Under these conditions a matrix is formed from the SFP2.

A crucial step in the preparation of such nanostructured material is the preparation of core−shell particles with fluid cores. In recent years, encapsulation of fluid particles by rigid shells has stimulated great interest.[6,7−11] The best results were demonstrated for interfacial polymerization of a high-T_g polymer on the surface of a fluid low-T_g particles.[6,11,12] However, to achieve successful encapsulation of fluid polymeric particles, several conditions had to be fulfilled, which can be summarized as follows.

First, a good compatibility between the core- and shell-forming polymers has to be provided in order to synthesize particles with a core−shell structure. Depending on the interfacial tension between a CFP and a SFP, composite latex microbeads can exhibit morphologies varying from complete phase separation or raspberry, mushroom, and "acorn" shapes to uniform SFP coatings on the surface of the latex cores[13,14] The compatibility between CFPs and SFPs is generally enhanced by modifying the compositions of the constituent polymers,[6] by using compatibilizers,[15] or by employing grafted macromonomers in the synthesis of the SFP.[16]

The second problem in the preparation of core−shell latex particles is the mutual diffusion of the core- and shell-forming polymers, which counteracts the formation of a distinct core−shell structure. The diffusion can be suppressed by cross-linking of the CFP and/or the SFP, which also leads to more advanced phase separation in the core−shell particles.[9] Obviously, in our approach the degree of cross-linking of the CFP should be very low when synthesis of the core−shell particles with fluid cores is a priority.

Third, the collapse of core−shell particles with fluid cores during particle synthesis and especially during film formation may be a serious obstacle when these particles are used as structural blocks for the preparation of nanocomposite films. The collapse of the cross-linked rubbery shells on the surface of fluid polymeric cores has been recently reported by Antonietti et al.[12] The authors found that a reduction in the cross-linking density of the SFP suppresses the collapse of the liquid cores.

Finally, since our ultimate objective was to use fluid cores as containers for optically sensitive species, we aimed at synthesis of core−shell particles with a minimum possible shell 1 thickness (see Figure 1), i.e., with the maximum ratio between the diameter of the fluid cores and the thickness of the inert rigid shell.

The results of our work are presented in two articles. Here, we focus on the synthesis of the building blocks of the nanostructured material, i.e., core−shell particles with a fluid core and a thin rigid shell synthesized from the SFP1. In the following paper,[17] we report on the nanocomposite material produced from the core−shell particles composed of CFP + SFP1 + SFP2.

Both the CFP and the SFP1 were synthesized from the copolymers of poly(butyl acrylate) (PBA) and poly(methyl methacrylate) (PMMA) with a different weight ratio PBA/PMMA in the CFP and the SFP. The encapsulation of the fluid cores was examined in different stages of the shell synthesis. We found that an optimum ratio PBA/PMMA in the SFP exists, which provides the formation of the thin shell uniformly covering the fluid core in early stages of the shell synthesis. The phenomenon of collapse of the rigid shells was suppressed by increasing the degree of cross-linking of the SFP. The factors leading to crack formation and collapse of the rigid SFP1 are discussed and evaluated.

Experimental Section

Materials. Methyl methacrylate (MMA, 99%) and butyl acrylate (BA, 99%) monomers (Aldrich, Canada) were purified by distillation under reduced pressure. Ethylene glycol dimethacrylate (EGDMA, Aldrich, 98%) was used as supplied. The water was purified by distillation and deionized using the Millipore Milli-Q Plus purification system. The ionic initiator, potassium persulfate ($K_2S_2O_8$, Aldrich, 99%), the nonionic initiator 2,2′-azobis(2-methyl-propionitrile) (AIBN, Kodak, 99%), and the chain-transfer agent 3-mercaptopropionic acid 2-ethylhexyl ester (IOMP, TCI America, 98%) were used as received.

A fluorescent dye-labeled comonomer 4-amino-7-nitrobenzo-2-oxa-1,3-diazole-MA (NBD-MA) was copolymerized with the core-forming polymer, as published elsewhere.[1b]

Methods. Particle size distribution in different latex dispersions at different stages of synthesis was determined using a photocorrelation spectroscopy (PCS) technique (Zetasizer 3000HS, Malvern Instruments, UK).

A Hitachi S-570 scanning electron microscope was used to characterize the morphology of the core−shell particles. A droplet of a dilute latex dispersion was dried on the aluminum SEM stub and then coated with a thin gold layer under pressure (10^{-5} Torr). The accelerating voltage was 15 kV, and the working distance used was 15 mm.

The glass transition temperatures of the CFP and the SFP in both homogeneous and composite particles were examined on a Perkin-Elmer DSC-7 differential scanning calorimeter under a nitrogen atmosphere at a heating rate of 10 °C/min.

Latex Synthesis. The core−shell latex particles were synthesized via two-stage polymerization using a semicontinuous reaction scheme. A mixed ionic−nonionic initiator approach was used, as is described elsewhere.[18] Both the liquid cores and the rigid shells were synthesized from a copolymer of PBA and PMMA with a different PBA/PMMA ratio in the CFP and the SFP. In the first stage, polymerization was initiated by the ionic initiator potassium persulfate, whereas the nonionic initiator AIBN was used in the second stage, providing growth of the existing latex microbeads and minimizing the probability of nucleation and growth of the secondary particles.

All reactions were carried out in a three-neck flask at 80 ± 0.1° C. The flask was equipped with a condenser, mechanical stirrer, and inlets for nitrogen and monomer. Prior to polymerization, the reaction mixture was purged with nitrogen, and a small positive pressure of nitrogen was maintained during the synthesis.

The PMMA−PBA core particles were synthesized in stage 1, and their composition was maintained constant. Deionized water (35 mL) and potassium persulfate (0.1 g) were precharged into the reaction vessel and heated to the reaction temperature 80 ± 0.2 °C. A monomer mixture containing 6 g of MMA, 9 g of BA, 0.067 g of IOMP, 0.45 g of EGDMA, and 0.008 g of the fluorescent comonomer NBD-MA was fed to the reactor via a fluid metering pump for about 3−4 h. After completing the addition of the monomer mixture, the flask contents were stirred for 1 h to complete the reaction.

Hard nonfluorescent PMMA−PBA shells were polymerized on the surface of the soft latex particles in stage 2. About 10 g of the latex dispersion from stage 1 and 35 mL of water were mixed in the reaction vessel to provide the solid content of the mixture of ca. 6.7 wt %. Then, 6 g of a monomer mixture containing MMA, BA, EGDMA, IOMP, and AIBN was pumped into the reaction flask under stirring at the rate of ca. 0.01−0.05 mL/min. In the first series of experiments, the concentration of the cross-linking agent EGDMA was varied from 0 to

Table 1. Glass Transitions of Individual Polymers and Polymers Incorporated in Core−Shell Structures

N	particle morphology	CFP[a]	SFP	exptl $T_{g,core}/T_{g,shell}$, °C, if any	calcd $T_{g,core}/T_{g,shell}$, °C, if any [b]
1	homogeneous	PMMA/PBA 40/60		−1.6/−	−3/−
2	homogeneous	PMMA		129/−	125/−
3	core−shell	PMMA/PBA 40/60	PMMA	1.5/123.5	−3/125
4	core−shell	PMMA/PBA 40/60	PMMA/PBA 95/5	3.6/107.5	−3/109

[a] CFP and SFP were cross-linked by 1.5% EGDMA and the CFP contained NBD dye. [b] T_g's of copolymers were calculated using the Fox equation.

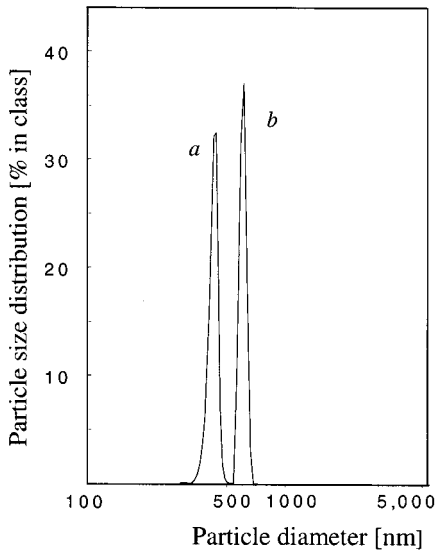

Figure 2. Size distribution curves for core particles (a) and core−shell particles (b) measured by photocorrelation spectroscopy. Polydispersity index measured by PCS: 0.04 (a) and 0.2 (b).

1.5, 2.5, 9, or 15 mol %, while keeping the composition of the SFP1 constant. In the second series of experiments, the concentration of EGDMA was maintained constant, whereas the weight fraction of PBA in the SFP1 was 0, 0.05, 0.1, or 0.2. For example, for the 5 wt % fraction of PBA in the SFP1, the monomer mixture contained 14.25 g of MMA, 0.75 g of PBA, 0.45 g of EGDMA, 0.95 g of AIBN, and 0.067 g of IOMP. Following the addition of the monomer mixture, small amounts of the latex dispersion were withdrawn from the reaction flask, and the morphology of the latex particles during shell synthesis was analyzed with SEM.

Results

Fluid Latex Cores. The weight ratio PBA/PMMA in the CFP was 1.5:1 and did not change in the course of experiments. Figure 2, curve a, shows particle size distribution as determined by PCS for the fluid latex cores. The average diameter of the particles was 420 nm, and the polydispersity index measured by PCS was 0.04. The T_g of the CFP for the noncoated core particles was −1.6 °C (see Table 1). This value is close to T_g = −3 °C, which was calculated for the PBA−PBMA copolymer using Fox equation, for $T_{g,PBA}$ = 218.2 K[19,20] and $T_{g,PMMA}$ = 402.2 K.[21]

Latex Shells. The synthesis of rigid shells on the surface of fluid cores was studied as a function of several parameters. First, the weight ratio PBA/PMMA in the SFP denoted as ϕ was varied from 0 to 0.25. Second, the weight ratio SFP1/CFP designated as φ was varied from 0 to 2.0. Third, the concentration of the EGDMA agent in the SFP1 changed from 0 to 15 mol %, determining the extent of cross-linking of the SFP1.

Following an increase in φ, the mean diameter of the core−shell particles gradually increased and for φ = 2.0 reached 620 nm; i.e., the average thickness of the shells was about 100 nm. The size distribution of the core−shell particles was broader than that for the core particles, as is shown in Figure 2, in contrast with the high monodispersity of composite latex particles with rigid cores.[1]

To study the change in particle morphology during the synthesis of the latex shells, the structure of the core−shell microspheres in different stages of shell synthesis was examined with SEM. Figure 3 shows typical images of the core−shell particles obtained during synthesis of the SFP1. The vertical columns show the change in particle morphology when φ increases from 0 to 2.0, whereas the horizontal rows demonstrate particle morphology for ϕ ranging from 0 to 0.25.

The intrinsic feature of the images shown in the horizontal rows is the existence of the optimum composition of the SFP1, for which a rigid shell protects a fluid core from spreading on the solid substrate. This effect is best demonstrated for φ = 1.33 (Figure 3, top row, left to right). When SFP1 is synthesized from PMMA, the soft cores do not maintain their spherical shapes. The latex particles coalesce and form a film on the solid substrate; however, no complete spreading of the fluid CFP occurs on the surface of the SEM stub, and the contours of individual particles can be still resolved, as is shown in Figure 3a. A similar image was obtained for individual latex cores, i.e., for φ = 0. In contrast, when ϕ increases to 0.05, the shape of the core−shell particles becomes spherical and spreading of the CFP is suppressed (Figure 3b), although the liquid necks between the microspheres can be resolved. Further increase in ϕ to 0.25 again leads to spreading of the CFP on the solid substrate, as is shown in Figure 3c.

Following an increase in φ (Figure 3, top to bottom), the composite latex particles gradually acquire a spherical shape. However, for different values of ϕ, complete particle coating with the SFP1 occurs for different weight ratios SFP1/CFP.

Comparison of the images in the second row of Figure 3 (φ = 1.67) shows that for ϕ = 0 (Figure 3d) individual core−shell latex particles can be resolved; yet, their surfaces are sticky, since the CFP is leaking through the incomplete shells. For ϕ = 0.05 (Figure 3e) the spherical core−shell particles have sharp nonsticky boundaries, while for ϕ = 0.25 (Figure 3f) the particle morphology is similar to that in Figure 3d. In the bottom row of Figure 3 for φ = 2.0, all core−shell particles achieve a spherical shape and sharp boundaries.

For all core−shell particles shown in Figure 3, a small number of undersized particles were observed. This effect will be discussed later.

The fact that two distinct glass transition temperatures were measured for the composite latex particles is a good indication of the core−shell structure of the latex microspheres synthesized from the slightly cross-linked CFP and SFP1. (A detailed spectroscopic com-

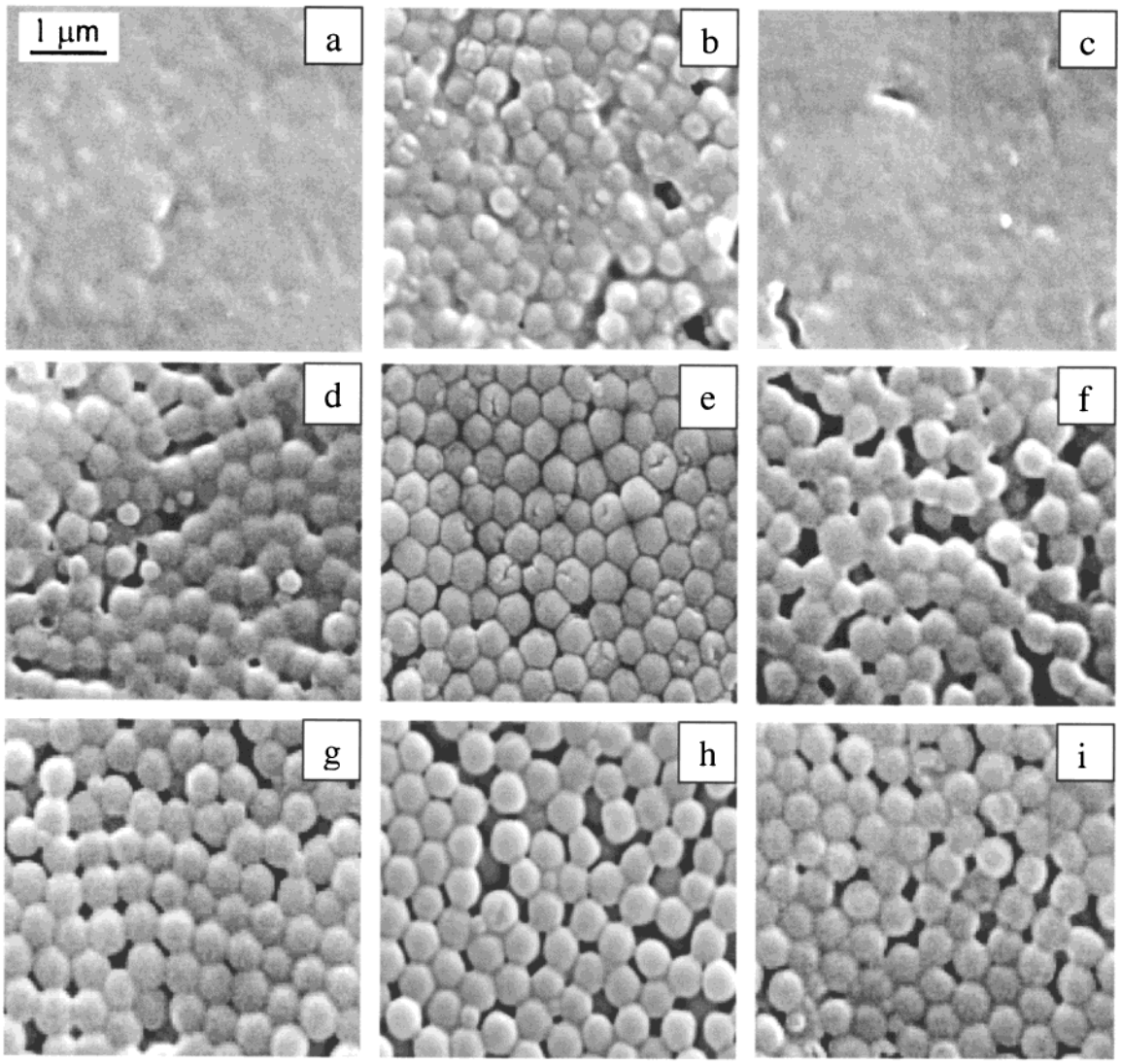

Figure 3. Typical SEM images of thecore−shell particles showing evolution in particle morphology during synthesis of the latex shells. In horizontal rows the weight ratio CFP/SFP1, φ, is maintained constant, whereas $\varphi = 1.33$ (a−c); $\varphi = 1.67$ (d−f); and 2.0 (g−i). In vertical columns the weight fraction of PBA, ϕ, is constant, while ϕ: 0 (a, d, g); 0.05 (b, e, h); 0.25 (c, f, i). $c_{EGDMA} = 2.5$ mol. %. Scale bar is 1 μm.

positional characterization could shed more information on the extent of mixing in the interfacial core−shell region.[9]) In Table 1, the reference glass transition temperatures −1.6 and 129 °C are given for the homogeneous latex particles synthesized from the CFP and from the cross-linked PMMA only (samples 1 and 2, respectively). In the core−shell particles obtained for $\phi = 0$ (sample 3), $T_{g,CFP} = 1.5$ °C and $T_{g,SFP1} = 123.5$ °C. These values are close to the T_g's of the corresponding reference samples 1 and 2, respectively. Similarly, in the composite particles with $\phi = 0.05$, the values of the glass transition temperatures are 3.6 and 107.5 °C for the CFP and the SFP1, respectively, which agrees well with the calculated values of T_g's of these polymers. In addition, the value 3.6 °C is relatively close to −1.6 °C, measured for the CFP in the homogeneous particles (sample 1). A slight shift in the values of the $T_{g,CFP}$ and $T_{g,SFP}$ toward each other (in comparison with the T_g's of the reference samples) may originate from weak mutual diffusion of the CFP1 and the SFP, which occurs in the core−shell particles despite polymer cross-linking.

Upon careful examination of the core−shell particles in Figure 3, it was found that a substantial number of the core−shell particles had collapsed. This phenomenon was further studied for the core−shell particles obtained for $\phi = 0.05$. In these latex systems two types of coexisting collapsed microbeads were found. The first type of defects is demonstrated in Figure 4a. For $\varphi = 1.67$, i.e., in the early stages of shell synthesis, spherical-like cracked particles were observed, which had approximately the same dimensions as the intact microspheres. In the later stages of the SFP1 synthesis, i.e., for $\varphi = 2.0$, the cracks were partly "healed"; i.e., their size and depth decreased, as is shown in Figure 4b. The "scars" remaining on the surface of core−shell particles could be ultimately healed by synthesizing thicker rigid shells.

The second type of collapsed core−shell particles is shown in Figure 4c. These particles have a significantly smaller size than the rest of the microbeads and are presumably the source of the higher polydispersity obtained for the core−shell particles. The collapsed particles are not spherical but have a "clam" structure. The contrast between the particle contents and the shell is high, which results from the release of the fluid CFP into the surrounding medium.

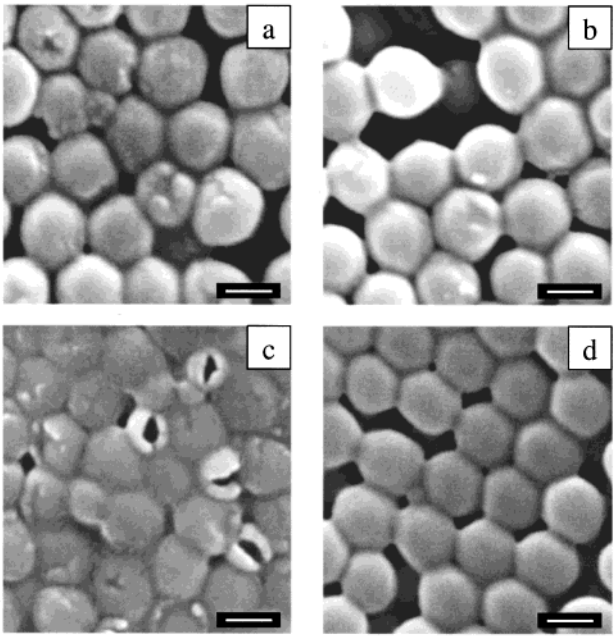

Figure 4. Morphology of the core−shell particles synthesized with different amounts of the cross-linking agent, c_{EGDMA}, in the SFP1. (a) $c_{EGDMA} = 1.5$ mol %, $\phi = 0.05$; $\varphi = 1.67$; (b) $c_{EGDMA} = 1.5$ mol %, $\phi = 0.05$; $\varphi = 2.0$; (c): $c_{EGDMA} = 2.5$ mol %, $\phi = 0$; $\varphi = 2.0$; (d) $c_{EGDMA} = 9$ mol %, $\phi = 0$; $\varphi = 2.0$ (d).

The phenomenon of the collapse of the latex shells was studied as a function of the extent of cross-linking of the SFP1. The concentration of the cross-linking agent in the SFP1 was varied from 0 to 1.5, 2.5, 9.0, or 15 mol %. It was found that when the concentration of EGDMA, c_{EGDMA}, reaches 9.0 mol %, both types of particle defects are suppressed. Figure 4d shows a typical morphology of the core−shell particles for $\varphi = 2.0$, $\phi = 0.05$, and $c_{EGDMA} = 9$ mol %. Particle monodispersity in this system is substantially higher than that in the latex dispersions obtained for the lower values of c_{EGDMA}. Second, all composite particles have a spherical shape, and their surfaces are free of cracks or any other types of defects. A similar structure of the composite particles was observed for $c_{EGDMA} = 15$ mol %.

Another important feature observed for the varying concentrations of EGDMA was the effect of the extent of cross-linking on the critical ratio of SFP1/CFP, for which the core−shell microbeads maintained their spherical shape. The variation of the critical value of SFP1/CFP with c_{EGDMA} is shown in Figure 5. When c_{EGDMA} increased from 0 to 15 mol %, the critical ratio SFP1/CFP decreased from 2.0 to 0.67.

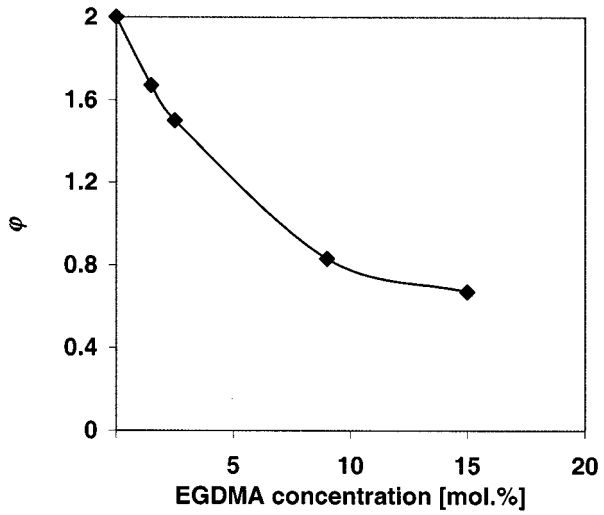

Figure 5. Effect of the concentration of the cross-linking agent on thecritical ratio SFP1/CFP required to protect the liquid cores from spreading. $\phi = 0.05$.

Discussion

Effect of Composition of SFP1 on Morphology of Core−Shell Particles. Since both the CFP and the SFP1 were cross-linked and the glass transition temperatures of these polymers in the composite latex particles were reasonably close to those of the individual constituent polymers, we assumed that polymer diffusion of the polymers between latex cores and shells was to the large extent suppressed. Under these conditions, there are two possible reasons for the spreading of the fluid CFP on solid surfaces, as shown in Figure 3a−c for the early stages of shell synthesis.

In the first instance, when the SFP1 is synthesized from PMMA ($\phi = 0$) and there is a substantial difference in interfacial tension between the CFP and the SFP1, encapsulation of the fluid cores occurs through the nucleation of the small PMMA particles adhering to the PBA/PMMA core.[6,22] For $\varphi = 1.33$ the surface of the latex cores is covered by scarce PMMA clusters with the height and diameter of ca. 26 and 30 nm, respectively.[22] As a result, the fluid core particles do not maintain their spherical shape and spread on the SEM stub. When the concentration of PBA in the SFP1 increases to $\phi = 0.05$ and then to $\phi = 0.1$, the compatibility between the CFP and the SFP leads to coating of the liquid cores with a dense layer of the SFP1, whereas $T_{g,SFP1}$ is sufficient to support the spherical shape of particles. However, upon further increase in ϕ to 0.25, partial spreading of the CFP occurs again, despite the enhanced compatibility of the CFP and the SFP1 and a relatively high value of $T_{g,SFP1} = 71$ °C calculated for $\phi = 0.25$. This effect can be explained either by the enrichment of the SFP1 with PBA or by a gradient in concentration of PBA in the latex shell. Both effects need further investigation.

Following an increase in the ratio SFP1/CFP, the degree of surface coverage of the fluid cores with the SFP1 increases. For example, for $\varphi = 1.67$ and $\phi = 0$ (Figure 3d), the clusters of PMMA merge to form a shell, which supports a spherical shape of the core−shell particles, but is not complete enough to prevent partial leakage of the CFP (Figure 3d). For $\varphi = 2.0$ the shell formation is complete, although particle surfaces remain somewhat sticky (Figure 3g). For $\phi = 0.05$ and 0.1, the SFP1 densely covers the fluid cores in the earlier stages of the shell synthesis, and for $\varphi = 1.67$ the thickness and the density of the latex shells are sufficient to preserve the spherical shape of the core−shell particles.

Table 2 summarizes the effect of the interrelationship between ϕ and φ in the synthesis of the core−shell particles with fluid cores. The earliest encapsulation of the fluid cores, characterized by the well-defined spherical shape of the core−shell particles and the absence of stickiness, occurs for $\phi = 0.05$ and $\phi = 0.1$, whereas for $\phi = 0$ and for $\phi = 0.25$ encapsulation occurs only in late stages of the SFP1 synthesis for $\varphi = 2.0$. Thus, for $\phi = 0.05$ and for $\phi = 0.1$, the thinnest rigid shells can be obtained in the composite particles, whose thickness calculated from the corresponding of φ is ca. 0.9 of that obtained for $\phi = 0.1$ and for $\phi = 0.2$.

Table 2. Minimum Weight Ratio SFP1/CFP Supporting Spherical Shape of the Core−Shell Particles with Fluid Cores[a]

	φ			
ϕ	0	0.05	0.1	0.25
1.33	S	L	L	S
1.67	L	P	P	L
2.0	P	P	P	P

[a] S = spreading of the fluid cores on the solid substrate; L = core−shell particles maintain a spherical shape but leakage of the CFP occurs through the shell; P = core−shell particles have sharp nonsticky boundaries.

Overall, for a particular value of ϕ the main features of the evolution of particle morphologies are consistent with the schematic representation given by El-Aasser et al.[6]

Cracking and Collapse of the Core−Shell Particles. The defects observed in the core−shell particles can be generated by two different mechanisms. The presence of "slits" on the surface of the average size particles in Figure 4a is explained by an incomplete coverage of the liquid cores with the SFP1 in early stages of shell synthesis. When φ reaches 2.0, the "slits" become smaller and for large values of φ can be ultimately "healed".

The second type of defects originates from the cracking and collapse of the core−shell particles. This phenomenon has been observed by several groups,[7,10,12,23] when liquid particles, not necessarily of a polymeric nature, were encapsulated with rigid polymeric shells. Several reasons for the collapse of the latex shells have been suggested, which have included interfacial tension gradients during synthesis,[23] capillary forces acting between particles when the latex dispersion was dried under ambient conditions,[12] and the use of high vacuum in SEM experiments.[10] In addition, the collapse of a rigid latex shell could occur during cooling of the latexes from the reaction temperature down to the room temperature due to the different thermomechanical properties of the CFP and SFP. In principle, the collapse of the rigid shells can be dominated by different factors in different stages of the preparation of core−shell microspheres.

The cooling of the latexes after synthesis, the action of capillary forces during latex drying, and the evacuation of air in the preparation of samples for SEM all have the same effect on the core−shell particles: they produce pressure gradients in the latex shells. As an example, we will discuss the effect of latex cooling; however, it can be expected that the proposed approach to the evaluation of pressure gradients in latex shells is applicable to other situations as well.

Because of the different thermoexpansion coefficients of the CFP and the SFP1 upon latex cooling from ca. 80 to ca. 22 ± 2 °C, the cores and shells in the composite particles undergo different degrees of shrinking; therefore, a pressure gradient is generated in the shell. The factors favoring the pressure gradients in the SFP1 include (i) the difference in thermoexpansion coefficients of the CFP and SFP1, (ii) the chemical attachment of the SFP1 to the surface of the CFP, and (iii) the rigid nature of the SFP1.

Figure 6 gives a two-dimensional schematic of a core−shell particle. Let r_c, l_s, and R be the radius of the liquid core, the thickness of the rigid shell, and the radius of the core−shell particle, respectively, $l_s = R - r_c$. α_{CFP} and α_{SFP1} are the linear coefficients of thermal expansion of the CFP and SFP1, respectively; $\alpha = 1/l\ (\partial l/\partial T)_P$, where l is the original linear dimension.[24]

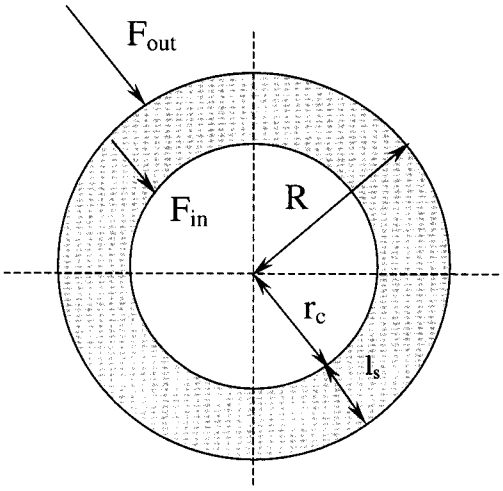

Figure 6. Schematic of forces imposed on a rigid shell in a core−shell particle with a fluid core.

Upon cooling, the reduction in r_c is

$$\Delta r_c = \alpha_{CFP} r_c \Delta T \tag{1}$$

where $\Delta T = T_{reaction} - T_{ambient}$, and the reduction in shell thickness is

$$\Delta l_s = \alpha_{SFP1} l_s \Delta T \tag{2}$$

When the latex core and shell shrink, a gradient in pressure, grad p, across the latex shell is

$$\text{grad } p = |P_{in} - P_{out}|/l_s \tag{3}$$

where P_{in} and P_{out} are the pressures imposed on the inner and the outer surfaces of the shell. Obviously, P_{in} is equal to the pressure on the surface of the particle core, while P_{out} is the pressure on the surface of the core−shell particle.

Let F_{in} and F_{out} be the radial forces acting perpendicular to the inner and outer surfaces of the latex shell and S_{in} and S_{out} be the surface areas of the latex cores and the core−shell particles, respectively; $S_{in} = 4\pi r_c^2$; $S_{out} = 4\pi R^2$.

Then

$$P_{in} = F_{in}/S_{in} \quad \text{and} \quad P_{out} = F_{out}/S_{out} \tag{4}$$

and

$$\text{grad } p = |F_{in}/4\pi r_c^2 - F_{out}/4\pi R^2|/l_s \tag{5}$$

It should be noted that a pressure gradient is a vector whose direction is determined by the relationship between the mechanical properties of the CFP and the SFP1. If $F_{in} > F_{out}$, the pressure vector is pointing from the center to the surface of the composite particle, and the latex shell would craze and "explode", whereas for $F_{in} < F_{out}$, the pressure vector is directed to the center of the particle and the shell would shrink and crack. Assuming an elastic response of the CFP and the SFP1 to deformation,[25] the value of F_{in} and F_{out} can be found as $F_{in} = E_{CFP}\Delta r_c/r_c$ and $F_{out} = E_{SFP1}\Delta l_s/l_s$, where E_{CFP} and E_{SFP1} are the Young's moduli of the CFP and SFP1, and $\Delta r_c/r_c$ and $\Delta l_s/l_s$ are the strains of the CFP and the SFP1, respectively.

Equation 5 can be rearranged as

$$\text{grad } p = |[E_{CFP1}\alpha_{CFP}r_c\Delta T/4\pi r_c^{\,3} - E_{SFP1}\alpha_{SFP1}l_s\Delta T/4l_s\pi R^2]|/l_s \quad (6)$$

and

$$\text{grad } p = \Delta T/4\pi l_s|[E_{CFP1}\alpha_{CFP}/r_c^{\,2} - E_{SFP1}\alpha_{SFP1}/R^2]| \quad (7)$$

Equation 7 shows that the pressure gradient in the SFP increases with the difference $T_{reaction} - T_{ambient}$ and with the thinning of the latex shell. Thus, the reduction in the shell thickness in composite latex particles has to be approached very cautiously. Second, grad p is at minimum when

$$(R/r_c)^2 \approx (E_{SFP1}\alpha_{SFP})/(E_{CFP}\alpha_{CFP}) \quad (8)$$

For the core−shell particles studied in the current work, $r_c = 210$ nm and $R = 310$ nm, and $(E_{SFP1}\alpha_{SFP1})/(E_{CFP}\alpha_{CFP})$ should be close to 2.2. In experiments described here, for $\phi = 0$ $E_{SFP1} = 3000$ MPa, $E_{CFP} \approx 1000$ MPa; $\alpha_{SFP1} = 2.0 \times 10^{-4}$ K^{-1},[26,27] and $\alpha_{CFP} \approx 5.8 \times 10^{-4}$ K^{-1} can be estimated using the empirical relation $\alpha_{CFP}T_{CFP} \approx 0.16$.[19] Thus, $(E_{SFP}\alpha_{SFP})/(E_{CFP}\alpha_{CFP}) \approx 1 < 2.2$. In such dispersions many core−shell particles with the "clam" morphology were observed.

Practically, the exact relation between the values of the Young's modulus and the thermoexpansion coefficients of the CFP and the SFP1, minimizing grad p in the latex shells, is unlikely. Under these conditions, collapse of the latex shells will depend on the fracture resistance of the SFP1. The suppression of cracking of the shells observed for the increased degree of cross-linking of the CFP1 results from a higher value E_{SFP1}.[19] Apparently, the extent of cross-linking achieved in the presence of 9 mol % of EGDMA provided sufficient fracture strength to the SFP1. In addition, cross-linking of the SFP1 led to the formation of a more compact shell structure on the surface of fluid cores and allowed us to prepare core−shell particles with thinner shells, which was one of the objectives of the current work.

It should be admitted that the alternative to increasing the fracture resistance of the SFP1 is in using elastomeric latex shells, which will deform easily in response to core shrinking or expansion. For such shells, stress relaxation in the shell-forming polymer will be determined by its elasticity, and an increase in cross-linking density will have a negative effect, as has been demonstrated by Antonietti et al.[12]

In summary, we examined the morphology of the core−shell latex particles with fluid cores and rigid shells as a function of the composition of the shell-forming polymer, the weight ratio core-forming/shell-forming polymer, and the concentration of the cross-linking agent in the shell-forming polymer. We found the optimum conditions under which monodispersed core−shell particles free of defects can be obtained. The factors leading to the collapse of the rigid particle shells were discussed and evaluated.

Acknowledgment. The authors are grateful to Nortel Networks for the financial support of this work. We thank Yongcai Wang for his assistance in DSC measurements. E.K. thanks Premier Excellence Research Award.

References and Notes

(1) (a) Kumacheva, E.; Noolandi, J.; Kalinina, O. Processes and Compositions. US Patent 5952131, 09/14/99. (b) Kumacheva, E.; Kalinina, O.; Lilge, L. *Adv. Mater.* **1999**, *11*, 231−234. (c) Kalinina, O.; Kumacheva, E. *Macromolecules* **1999**, *32*, 4122−4129.
(2) Vickreva, O.; Kalinina, O.; Kumacheva, E. *Adv. Mater.* **2000**, *12*, 110−112.
(3) Kalinina, O.; Kumacheva, E. *Chem. Mater.* **2001**, *13*, 35−38.
(4) Siwick, B. J.; Kalinina, O.; Kumacheva, E.; Miller, D. R. J. *J. Appl. Phys.*, in press.
(5) Talhavini, M.; Atvars, T. D. Z. *J. Photochem. Photobiol. A: Chem.* **1998**, *114*, 65−73.
(6) Kirsch, S.; Landfester, K.; Shaffer, O.; El-Aasser, M. S. *Acta Polym.* **1999**, *50*, 347−362.
(7) Loxley, A.; Vincent, B. *J. Colloid Interface Sci.* **1998**, *208*, 49−62.
(8) Berg, J.; Sundberg, D.; Kronberg, B. J. *Microencapsulation* **1989**, *6*, 317.
(9) Ishida, M.; Oshima, J.; Yoshinaga, K.; Horii, F. *Polymer* **1999**, *40*, 3323−3329.
(10) Ottewill, R. H.; Schofield, A. B.; Waters, J. A. *J. Dispersion Sci. Technol.* **1998**, *19*, 1151−1162.
(11) Dos Santos, F. D.; Fabre, P.; Drujon, X.; Meunier, G.; Leibler, L. *J. Polym. Sci., Part B: Polym. Phys.* **2000**, *38*, 2989−3000.
(12) Schellenberg, C.; Akari, S.; Regenbrecht, M.; Tauer, K.; Petrat, F. M.; Antonietti, M. *Langmuir* **1999**, *15*, 1283−1290.
(13) Dimonie, V. L.; Daniels, E. S.; Shaffer, O. L.; El-Aasser, M. S. In *Emulsion Polymerization and Emulsion Polymers*; Lowell, P. A., El-Aasser, M. S., Eds.; Wiley: Chichelston, 1997; Chapter 9, pp 293−3126.
(14) Rudin, A. *Macromol. Symp.* **1995**, *92*, 53−70.
(15) Wang, Z. Y.; Paine, A. J.; Rudin, A. *J. Polym. Sci., Part A: Polym. Chem.* **1995**, *33*, 1597−1606.
(16) (a) Nelliappan, V.; El-Aasser, M. S.; Klein, A.; Daniels, E. S.; Roberts, J. E. *J. Polym. Sci., Part A: Polym. Chem.* **1996**, *34*, 3173−3181. (b) Rajatapitu, P.; Dimonie, V. L.; El-Aasser, M. S.; Vratsanos, M. S. *J. Appl. Polym. Sci.* **1997**, *63*, 205−219.
(17) Kalinina, O.; Kumacheva, E., to be submitted in *Macromolecules*.
(18) Ocallaghan, K. J.; Paine, A. J.; Rudin, A *J. Appl. Polym. Sci.* **1995**, *58*, 2047−2055.
(19) *Encyclopedia of Polymer Science and Engineering*; Kroschwitz, J. I., Ed.; John Wiley & Sons: New York, 1985; Vol. 1.
(20) We assumed that $T_{g,SFP1}$ does not change significantly upon weak cross-linking.
(21) This value of T_g was experimentally measured for PMMA cross-linked at $c_{EGDMA} = 2.0$ mol %.
(22) Sommer, F.; Duc, T. M.; Pirri, R.; Meunier, G.; Quet, C. *Langmuir* **1995**, *11*, 440−448.
(23) Berg, J.; Sundberg, D.; Kronberg, B. *J. Microencapsulation* **1989**, *6*, 327−337.
(24) Here, we use linear coefficients of thermal expansion for simplicity, assuming that the CFP and SFP1 are isotropic and $\beta = 3\alpha$ where β is the bulk coefficient of thermal expansion.
(25) This is a reasonable assumption for the slightly cross-linked CFP, which in the temperature range varying from ca. 80 to 22 °C is in the rubbery state. For the glassy SFP1, a very small strain is assumed.
(26) *Encyclopedia of Polymers*; Kabanov, V. A., Ed.; Soviet Encyclopedia: Moscow, 1977; Vol. 1.
(27) *Polymer Handbook*, 3rd ed.; Brandrup, J., Immergut, E. H., Eds.; Wiley: New York, 1989.

MA0103472